BLANKET ENGINEERING

KEYWORDS: *fusion blanket neutronics, deuterium-tritium source, source characterization*

CHARACTERISTICS OF A DEUTERIUM-TRITIUM FUSION SOURCE ON A ROTATING TARGET USED IN SIMULATED FUSION BLANKET EXPERIMENTS

M. NAKAGAWA, T. MORI, K. KOSAKO, Y. OYAMA, Y. IKEDA, C. KONNO, H. MAEKAWA, and T. NAKAMURA
Japan Atomic Energy Research Institute, Department of Reactor Engineering
Tokai Research Establishment, Tokai-mura, Naka-gun, Ibaraki-ken 319-11, Japan

M. A. ABDOU *University of California, Los Angeles*
School of Engineering and Applied Science,
Mechanical, Aerospace, and Nuclear Engineering Department
Los Angeles, California 90095

E. F. BENNETT *Argonne National Laboratory, Fusion Power Program*
Building 205, 9700 South Cass Avenue, Argonne, Illinois 60439

M. Z. YOUSSEF *University of California, Los Angeles*
School of Engineering and Applied Science,
Mechanical, Aerospace, and Nuclear Engineering Department
Los Angeles, California 90095

T. YULE *Argonne National Laboratory, Fusion Power Program*
Building 205, 9700 South Cass Avenue, Argonne, Illinois 60439

Received January 28, 1994
Accepted for Publication July 28, 1994

The neutron source characteristics of the Japan Atomic Energy Research Institute (JAERI)/U.S. Department of Energy collaborative program on fusion neutronics Phase-IIA and -IIB experiments are determined by measuring neutron spectra and various activation rates in the cavity and on the inner surface of the enclosure and the test regions. The analyses are performed by both JAERI and the United States using individual nuclear data and transport codes. The neutron spectra are generally well predicted by both Monte Carlo and S_n calculations in the energy range of 15 MeV to a few kilo-electron-volts, except for energies 10 to 1 MeV. The discrepancies between the measured and the calculated activation rates are within ±10% when recently evaluated nuclear data are used. Through the present investigation, the characteristics of incident neutrons in the test region can be satisfactorily predicted.

I. INTRODUCTION

Blanket neutronics parameters were measured and analyzed by both the Japan Atomic Energy Research Institute (JAERI) and the United States for the Phase-II assembly. The assembly was constructed to simulate the blanket environment of a fusion reactor as much as possible. The neutron source and the Li_2O region were placed inside a Li_2CO_3 enclosure and a polyethylene layer to remove influence from the instruments, wall, etc., of the experimental room. In the Phase-IIA assembly, the test region of the reference system consisted of Li_2O, and in the Phase-IIB assembly, a 5-cm-thick beryllium zone was added at the inner surface of the test region and a Li_2CO_3 container. Many neutronics parameters were measured and analyzed in the test region, as described in related papers. To examine the prediction accuracy of blanket neutronics parameters, one should first confirm well the source characteristics. The prediction error of source characteristics propagates to errors of blanket parameters. For this purpose, neutron

spectra and various foil activation rates were measured around the rotating neutron target (RNT), with special care given at the front surface of the Li_2O test region. By using various activation foils with different threshold energies, one can evaluate the scattered component of the incident neutron current in the test region in addition to the uncollided direct deuterium-tritium (D-T) neutrons with energies of 13 to 15 MeV. This analysis is also useful for evaluation of activation cross sections.

This paper shows the results of comparison between the measurements and the calculations that were performed independently at JAERI (Ref. 1) and in the United States.[2] The nuclear data and calculation codes were the same as those used in the analysis of the test region. In the JAERI calculations, the DDL/J3 with 125 energy groups was used for transport calculations, which was processed from the JENDL3/PR1 file.[3] As activation cross sections, ENDF/B-IV, ENDF/B-V, and Fusion Neutronics Source (FNS) files were used. The last file involved recently measured data from the FNS facility.[4] Transport calculations were performed with the MORSE-DD Monte Carlo code,[5] which is a modified version of MORSE-CG. The code uses a multigroup double-differential cross section and, hence, can accurately treat the anisotropy in the elastic and inelastic scattering process by considering kinematics. The United States used the RMCCS/BMCCS library based on ENDF/B-V for the MCNP 3A calculations.[6] The MATXS6 library[7] was used for the DOT5.1 discrete ordinates calculations. For activation cross sections, the ACTL library compiled at Los Alamos National Laboratory was adopted.

Fig. 1a. Photograph of RNT.

II. NEUTRON SOURCE GENERATION

The neutron source used in the experiments was generated based on a $^3T(d,n)^4He$ reaction. The accelerated D^+ beam bombarded the tritiated titanium coated on the copper plate of RNT, which is shown in Fig. 1a. The target was cooled with water. Figure 1b shows the calculation model used in the present MORSE-DD analysis. The model was slightly different between JAERI the United States. The actual RNT had a more complicated structure. Bombarding deuterons were slowed down to zero energy in the titanium coating. During this process, neutron generation reactions were possible at various energies. Accordingly, the energy of the emitted neutrons depended on that of the deuterons, although such dependence was small because emitted neutron energy was ~14 MeV compared with ~300 keV for deuterons. Nevertheless, such energy dependence was taken into account in the Monte Carlo calculations based on Ref. 8 where the reaction probability table is given, corresponding to the deuteron energy.

The angular distribution of emitted neutrons is almost isotropic in the center-of-mass (c.m.) system, but

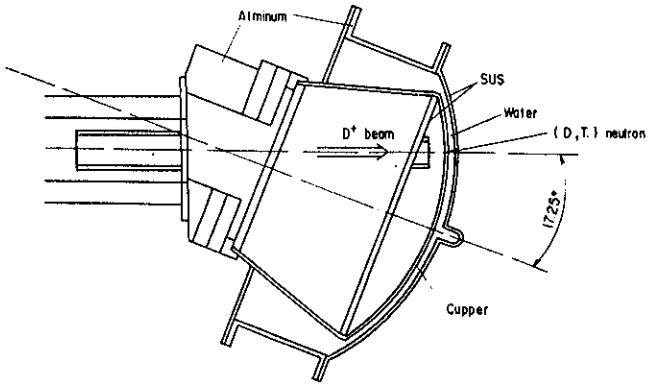

Fig. 1b. Cross-sectional view of RNT (calculation model).

an anisotropy effect was considered by using the experimental formula given by Benveniste et al.[9] as follows:

$$\frac{\sigma(\theta_n)}{\sigma(0)} = 0.998 + 0.0213 \cos\theta_n - 0.0190 \cos^2\theta_n \ ,$$

which is given for incident deuterons at $E = 350$ keV. An emission angle in the c.m. system θ_n was sampled from this formula.

After determination of E_1 and θ_n, an emission angle ϕ_n in the laboratory system was obtained by the following relation:

$$\sin\varphi_n = \pm\frac{\sin\theta_n}{(1+2\gamma\cos\theta_n+\gamma^2)^{1/2}}$$

(minus sign is taken if $\theta_n < -\gamma$)

or

$$\cos\varphi_n = \frac{\gamma+\cos\theta_n}{(1+2\gamma\cos\theta_n+\gamma^2)^{1/2}} ,$$

where

$$\frac{1}{\gamma^2} = \frac{m_a(m_1+m_2)}{m_n m_1}\left(\frac{m_2}{m_1+m_2}+\frac{Q}{E_1}\right)$$

m_1 = mass of incident deuteron

m_2 = mass of target triton

m_n = mass of neutron

m_a = mass of alpha particle

E_1 = incident energy of deuteron causing the reaction

Q = 17.6 MeV (total released kinetic energy).

Then, the emitted neutron energy in the laboratory system E_n was determined by the following formula by considering an effect of the relativistic theory:

$$E_n(E_1,\varphi_n) = W_n - m_n ,$$

where

$$W_n = \frac{1}{2a}\left[-b \pm (b^2-4ac)^{1/2}\right]$$

$$a = (W_1+m_2)^2 - (W_1^2-m_1^2)\cos^2\varphi_n$$

$$b = -(m_1^2+m_2^2+m_n^2-m_a^2+2m_2W_1)(W_1+m_2)$$

$$c = (m_1^2+m_2^2+m_n^2-m_a^2+2m_2W_1)/4 + m_n^2(W_1^2-m_1^2)\cos^2\varphi_n$$

$W_1 = m_1 + E_1$ = total energy of deuteron.

This calculation procedure was implemented in the MORSE-DD and the MCNP 3A Monte Carlo codes.

The calculated neutron source energy spectrum is shown in Fig. 2 for the angles to the z axis: $\theta = 0$, 60, and 120 deg. (The flight direction of the deuterons is along the z axis, and the azimuthal angle is presented as θ.) The normalized energy and the angular distribution of the neutrons are also presented in Table I.

III. SOURCE CHARACTERISTICS OF PHASE-IIA SYSTEM

The experiments for neutron source characterization were performed by measuring neutron spectra and

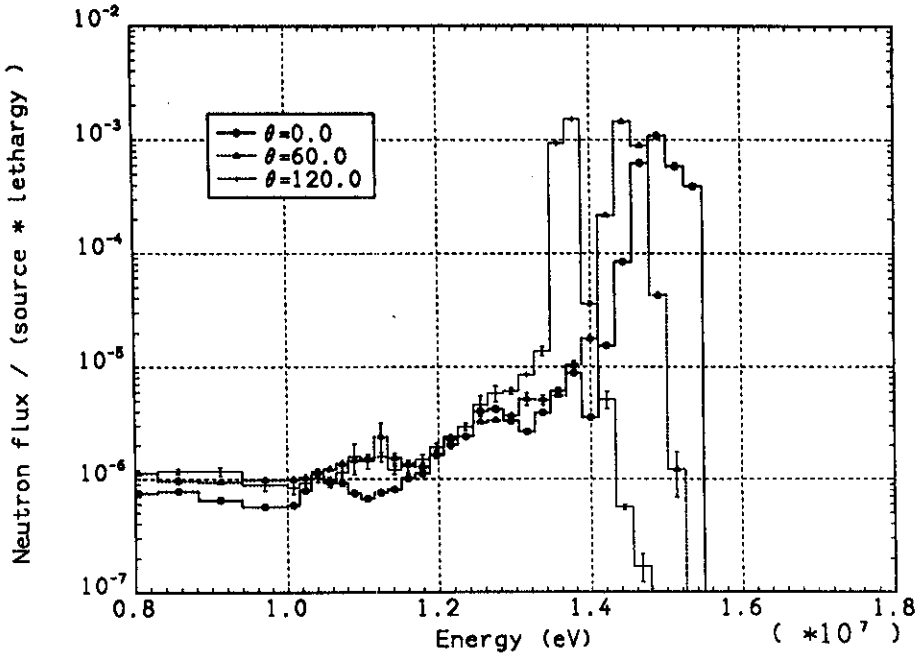

Fig. 2. The angular neutron spectrum from RNT. The distance from the neutron generation spot is 43.5 cm, and θ is the azimuthal angle to the z axis.

TABLE I

Energy and Angular Distribution of the Emitted (D-T) Neutrons

E (MeV) Upper	$S(u)$[a]	Angle $\mu = \cos\theta$[b]						
		−0.940	−0.707	−0.259	0.259	0.707	0.940	1.0
15.49	0.302						0.293	0.707
15.25	1.666					0.010	0.700	0.290
15.01	4.174					0.241	0.587	0.172
14.78	7.641					0.517	0.406	0.077
14.55	9.293				0.085	0.798	0.111	0.006
14.32	9.469				0.746	0.250	0.003	0.001
14.10	9.225			0.070	0.930			
13.88	8.882	0.001	0.033	0.939	0.027			
13.67	7.880	0.049	0.376	0.575				
13.46	4.313	0.184	0.698	0.118				
13.25	1.193	0.559	0.441					
13.04	0.031	1.0						
12.84								
Total[c]		0.028	0.108	0.215	0.260	0.233	0.123	0.032

[a]Energy distribution of source integrated for angle $\mu = \cos\theta$.
[b]θ is the angle with the D^+ beam.
[c]Normalized to unity.

foil activation rates in the cavity and on the inner surface of the container. The neutron spectrum was measured by an NE-213 counter, which is described in detail in Ref. 10, in the energy range above 1 MeV and by a proton recoil counter (PRC) below 1 MeV. The $^{58}Ni(n,2n)^{57}Ni$, $^{58}Ni(n,p)^{58}Co$, $^{93}Nb(n,2n)^{92}Nb$, $^{197}Au(n,2n)^{196}Au$, $^{197}Au(n,\gamma)^{198}Au$, and $^{27}Al(n,\alpha)^{24}Na$ reactions were used as activation foils. Virgin neutrons from RNT contributed to the high-energy component of the neutrons, and the low-energy component was from the scattered neutrons in the enclosure or the test region. Accordingly, by comparing measured neutron spectra or activation rates having various threshold energies to the calculated ones, a prediction accuracy could be evaluated for the direct and scattered components of the neutron current in the test region.

The test region of the reference system consisted of only a Li_2O zone, and the test region of the beryllium sandwich system[10] included a 5-cm-thick beryllium zone between the 5-cm-thick front and the 51-cm-thick rear Li_2O zones.

The measured and the calculated neutron spectra in the reference and the beryllium sandwiched systems are compared in Fig. 3, where the calculated source spectrum described in Sec. II was adopted. The calculated spectra by MORSE-DD were smeared over the detector energy resolution. The Gaussian function was used as the resolution function. The integrated spectra above 10 MeV agreed well with the measured spectra while the calculated 14-MeV peak seemed to be underestimated. The peak height itself was not so important in the present study because the uncertainty in the energy resolution of the measurement strongly influenced the peak height, which could not be accurately taken into account in the calculation. In the 1- to 10-MeV range, the discrepancies of a few tens percent, a factor 2, were observed, which could be caused from the uncertainty due to the unfolding technique for the NE-213 counter.[10] Below 150 keV, spectra by both calculation and by PRC agreed within the statistical uncertainties in most of the energy region for both systems, although a trend of slight overestimation was found below a few tens of kilo-electron-volts.

The results of the foil activation rates are discussed in the following. All the foils were placed at the midplane of the assembly, which was at the same level from the floor as that of the D-T source spot. The cross marks in Figs. 4 through 8 show the position of the foils placed. When the calculated-to-experiment (C/E) values are shown at each position, the upper ones are those calculated by using the ENDF/B-IV or ENDF/B-V cross sections, and the lower ones are those by the FNS file. The variances (1σ) of the Monte Carlo calculations are shown at the top of Figs. 4 through 8.

The result of the $Ni(n,2n)$ reaction is shown in Fig. 4 for the reference system. The C/E values based on the ENDF/B-IV data showed underestimation by

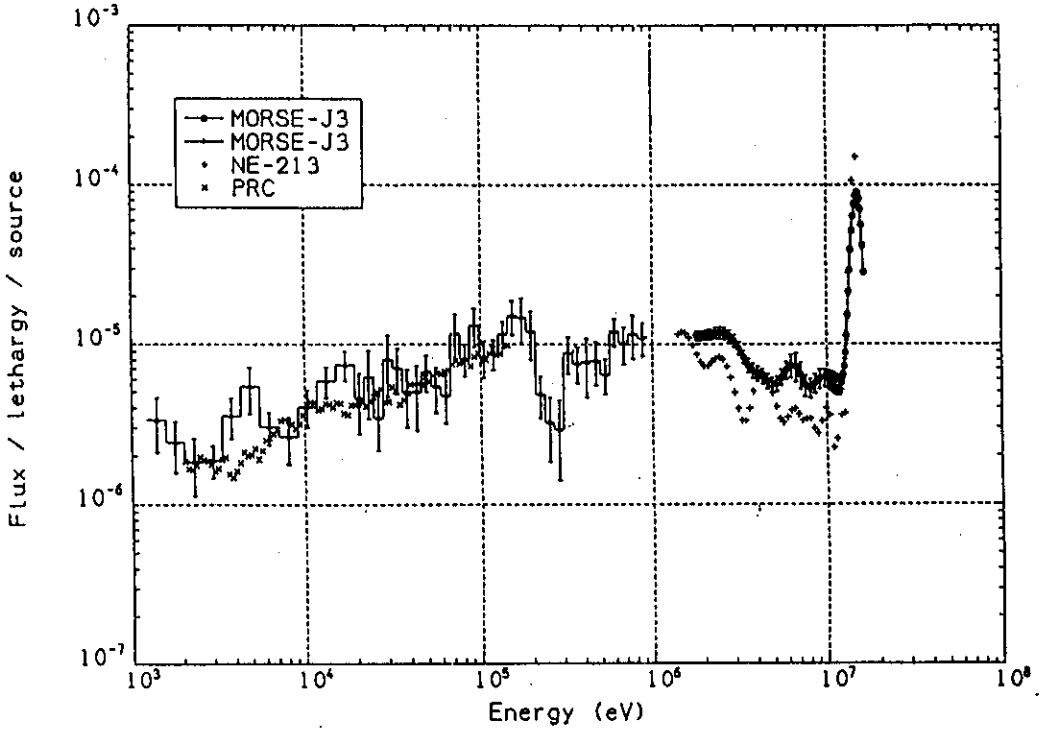

Fig. 3. The neutron spectrum at the front face of the test region in the Phase-IIA reference system.

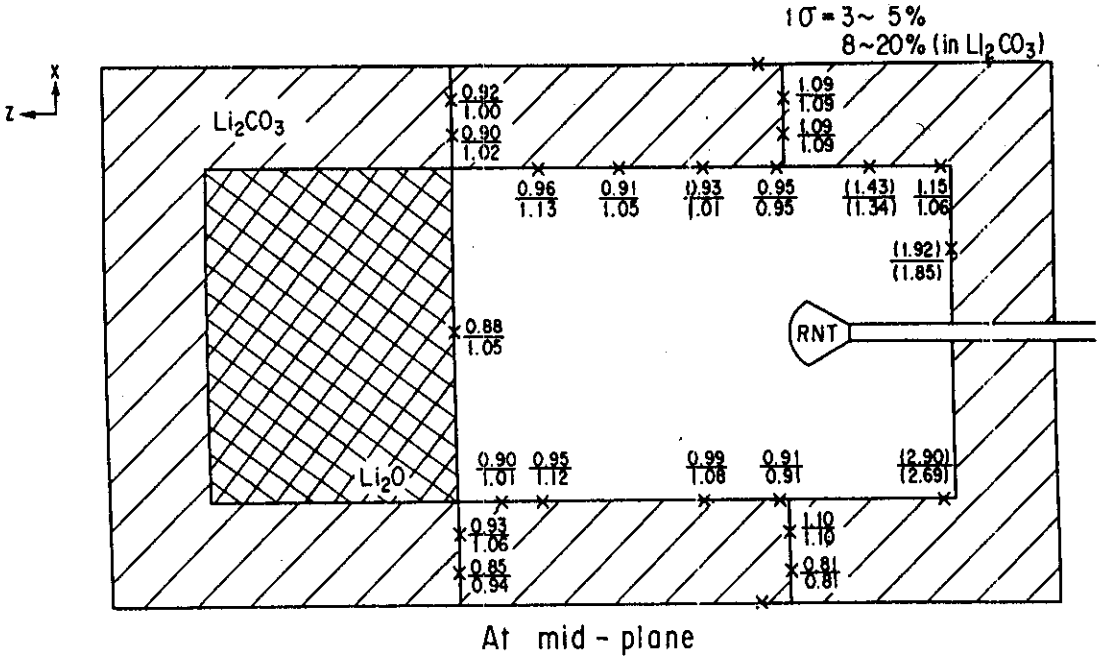

Fig. 4. The C/E values for the $^{58}Ni(n,2n)^{57}Ni$ reaction rate at the midplane of the Phase-IIA system (ENDF/B-V/FNS).

~10% in the forward direction from RNT, but the FNS file reduced the discrepancies to ~5%. At three locations, shown in parentheses, the calculations did not agree with the measured values. Such large deviations of the C/E values from unity were due to inaccurate modeling of the equipment that surrounds RNT (e.g., position and composition of a motor and cooling water tubes, etc.) which are placed at the back locations

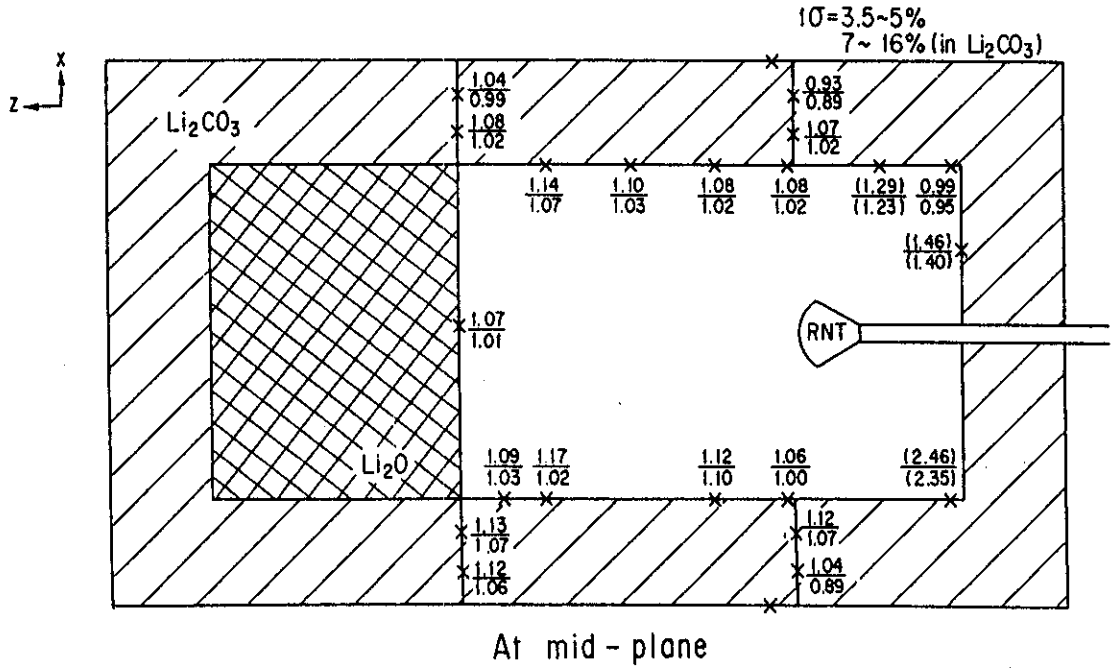

Fig. 5. The C/E values for the $^{93}Nb(n,2n)^{92}Nb$ reaction rate at the midplane of the Phase-IIA system (ENDF/B-IV/FNS).

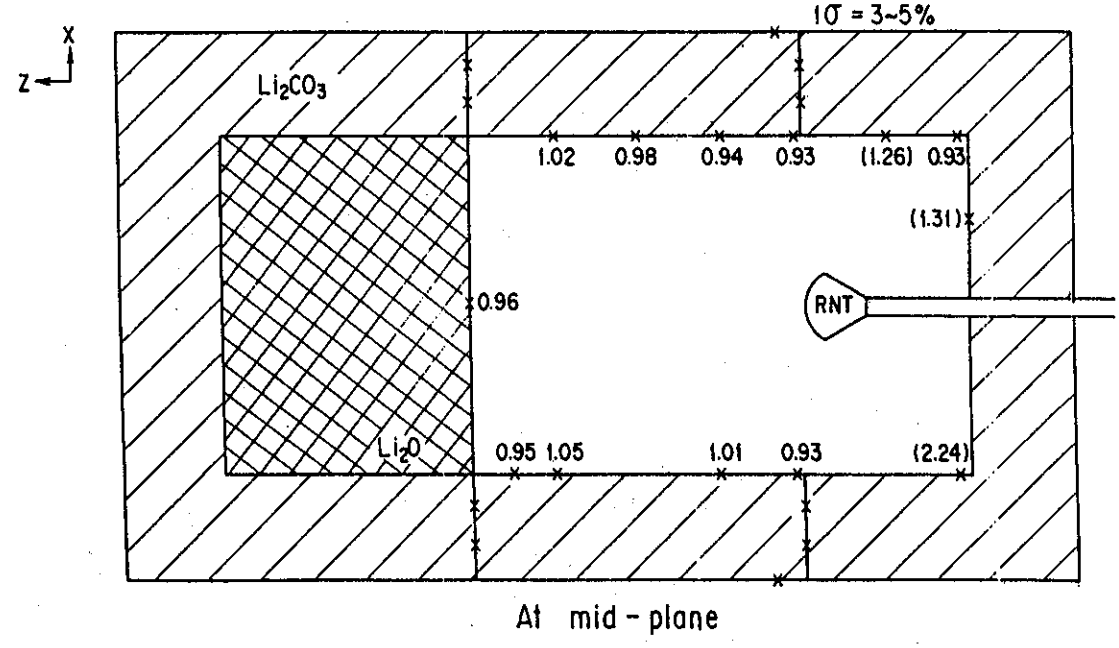

Fig. 6. The C/E values for the $^{197}Au(n,2n)^{196}Au$ reaction rate at the midplane of the Phase-IIA system (ENDF/B-V).

of RNT. Neutrons generated with a backward flight direction were scattered first by this equipment, and hence, the inaccuracy in modeling these components considerably affected the calculated reaction rates at these back locations, which were sensitive to high-energy neutrons. In spite of such discrepancies, the source characteristics in the forward direction were predicted with reasonable accuracy if recently measured activation cross sections were used, as seen in Fig. 4. In Fig. 5, the C/E values for the Nb(n,2n) reaction are shown. We found that ENDF/B-IV overestimated the reaction rates by several percent; on the other hand, the

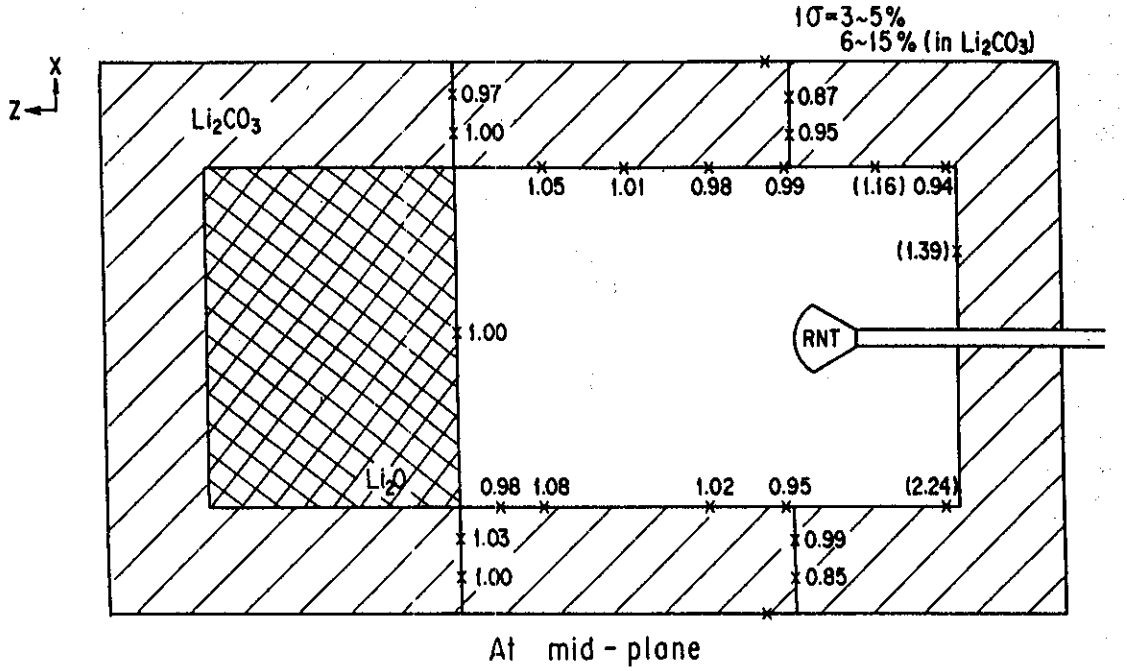

Fig. 7. The C/E values for the $^{27}Al(n,\alpha)^{24}Na$ reaction rate at the midplane of the Phase-IIA system (ENDF/B-V).

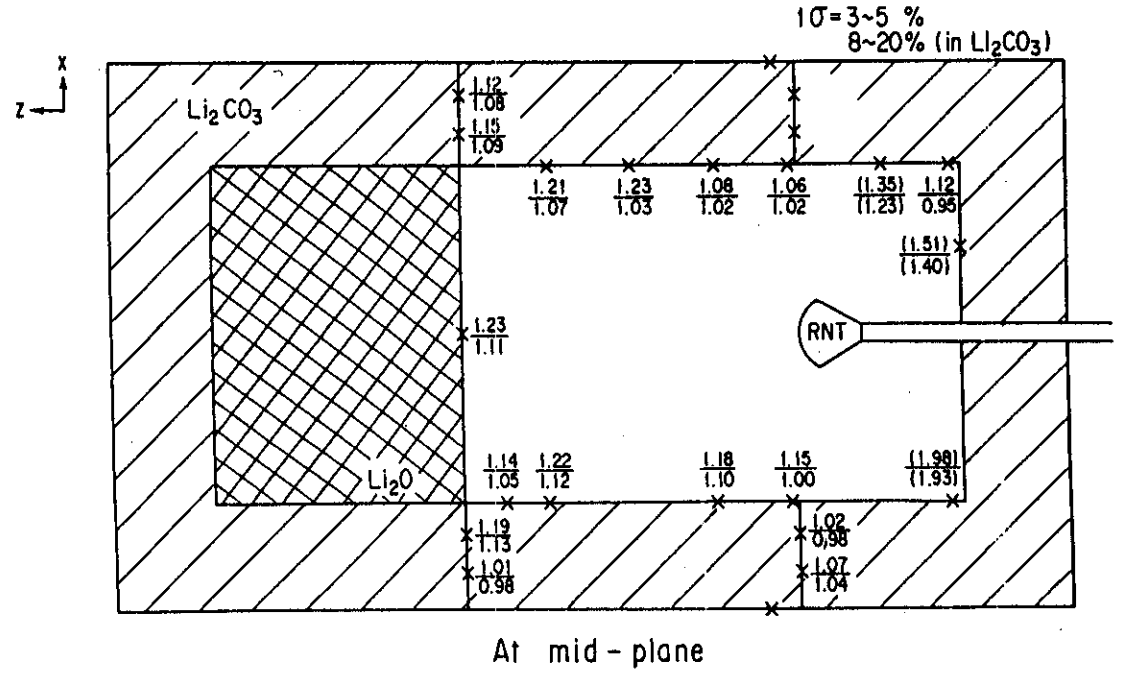

Fig. 8. The C/E values for the $^{58}Ni(n,p)^{58}Co$ reaction rate at the midplane of the Phase-IIA system (ENDF/B-V/FNS).

FNS file could predict those reactions fairly well. In the Li_2CO_3 container, the statistical uncertainty was large compared with that at the surface.

The map of C/E values for the $Au(n,2n)$ reaction rate is shown in Fig. 6, which shows that ENDF/B-V could predict well these reaction rates. Similar agreement was observed for the $Al(n,\alpha)$ reaction, as shown in Fig. 7. The accuracy of these two activation cross sections seemed to be satisfactory. Figure 8 shows the C/E values of the $Ni(n,p)$ reaction rates by the two files;

ENDF/B-V overestimated the values by ~20%, although the FNS file reduced the discrepancy significantly. We could see, however, a trend of overestimation from a few to 10%. Because this reaction had a relatively low threshold energy (~1 MeV), the reaction rates would be overestimated because of the overestimation of the neutron spectrum in the 1- to 10-MeV range, as mentioned earlier.

To examine the prediction accuracy of the incident source in the test region, we measured the activation rates described earlier at various positions on the surface of the test region. The foils were placed in horizontal and vertical directions with intervals of 10 cm. The C/E values for these reaction rates by MORSE-DD are shown in Figs. 9 through 14. Figures 9, 10, and 13 show two curves of the C/E values obtained by ENDF/B-IV or ENDF/B-V and the FNS file, respectively. The Ni$(n,2n)$ reaction rates calculated by the FNS file agreed well with the measurements in both directions. Such a trend was the same as the case in the other cavity region, as seen in Fig. 9. The Nb$(n,2n)$ reaction rates were also well predicted if the FNS file was used while ENDF/B-V overestimated them by ~10%, as seen in Fig. 10. The Au$(n,2n)$ and Al(n,α) reaction rates could be accurately predicted, as seen in Figs. 11 and 12, respectively. As to the Ni(n,p) reaction rates, ENDF/B-IV gave larger C/E values by 20% compared with unity, as seen in Fig. 13, while the FNS file fairly reduced the discrepancies. The C/E values were, however, still larger by 10% compared with unity at most locations. Figure 14 shows the C/E values by ENDF/B-IV for the Au(n,γ) reaction rates where those were smaller by 30 to 40% compared with unity, which was the same trend observed for the foils on the cavity wall. Such underestimation is partly attributed to the inappropriate homogenization model of epoxy paint (hydrogen-rich material) in the Li_2CO_3 container. By improving the model, the C/E values increased by 10 to 20%.

The C/E values obtained by the U.S. calculations based on MCNP and the RMCCS and the ACTL libraries are summarized in Figs. 15 and 16 for the horizontal and the vertical directions, respectively. The Ni$(n,2n)$ reaction rate was underestimated by ~15% in both directions, which was consistent with the result by JAERI using ENDF/B-IV. A trend of slight overestimation of the Nb$(n,2n)$ reaction rate was also similar between both teams. The U.S. calculation underestimated the Al(n,α) reaction rate while the JAERI calculation agreed well with the measurement. The JAERI calculation overestimated the Ni(n,p) reaction rate by ~10%; on the other hand, the U.S. calculation agreed well in the horizontal direction and overestimated or underestimated the measurement by several percent depending on the positions in the vertical one. Such discrepancies may primarily address the discrepancy in the neutron spectrum of 1 to 10 MeV.

Note that all the C/E values of the reaction rates were almost constant on the surface of the Li_2O test region, so the space dependence of the prediction accuracy for the incident neutrons was very small. In conclusion, one could say that through the present analysis of the neutron spectrum and the activation rates, the source characteristics of Phase-IIA could be well predicted by using the present calculation model, the MORSE-DD and MCNP Monte Carlo codes, and the recent activation cross sections except for the very low

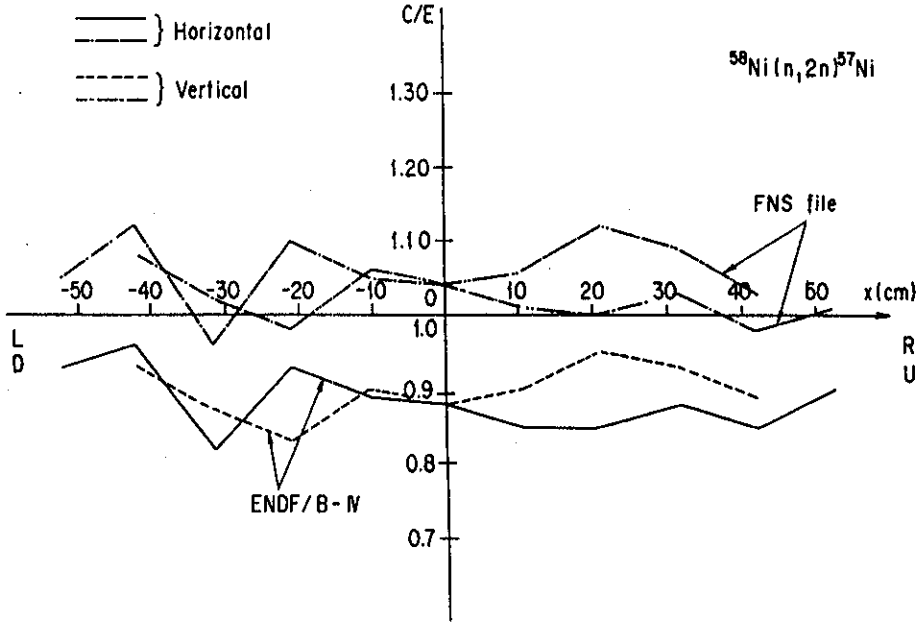

Fig. 9. The C/E values for the ^{58}Ni$(n,2n)^{57}$Ni reaction rate; $x = y = 0$ is the center of the test region surface.

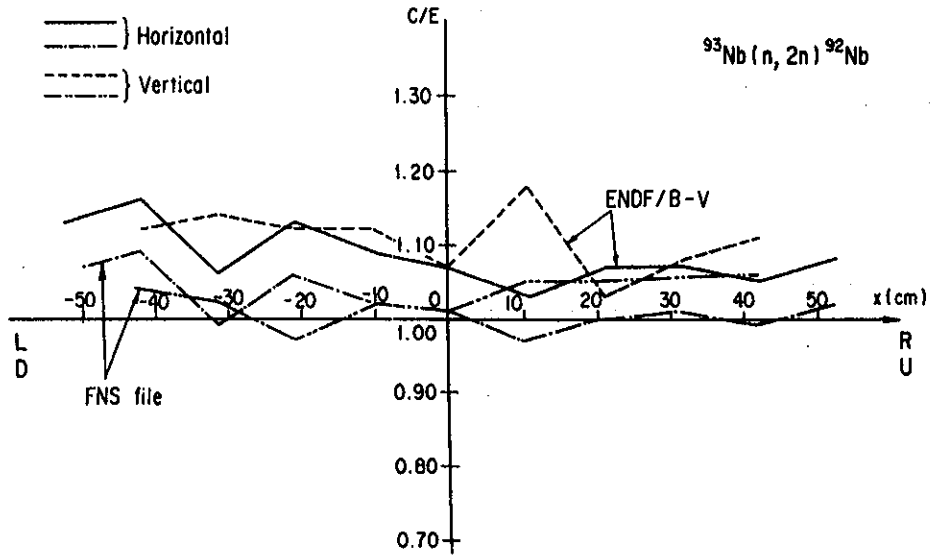

Fig. 10. The C/E values for the ^{93}Nb$(n,2n)^{92}$Nb reaction rate; $x = y = 0$ is the center of the test region surface.

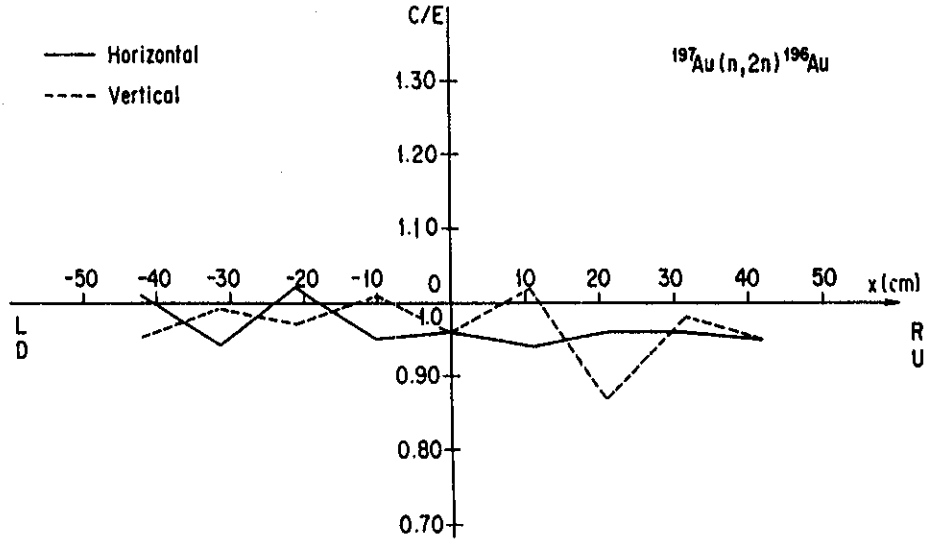

Fig. 11. The C/E values for the ^{93}Nb$(n,2n)^{92}$Nb reaction rate; $x = y = 0$ is the center of the test region surface.

energy component of the neutron spectrum, although uncertainty existed in the energy range 1 to 10 MeV.

IV. SOURCE CHARACTERIZATION OF PHASE-IIB SYSTEM

In the case of the Phase-IIB experiments, the source characterization was performed by measuring the foil activation rate by ^{93}Nb$(n,2n)^{92}$Nb and the neutron spectrum in the cavity region. Niobium foils were placed on the cross sections $\alpha - \alpha'$, $\beta - \beta'$, and $\gamma - \gamma'$ and on the front surface of the Li_2O test region, as shown in Fig. 17.

The neutron spectrum measured at the front of the test region [$x = y = 0$, z (distance from the front surface of the test zone)] is compared with the calculated neutron spectrum by JAERI in Figs. 18 and 19. The spectrum at the high-energy region above 1 MeV, which was measured by an NE-213 counter, is compared with the calculation in Fig. 18. Virgin neutrons generated by the D-T reaction made the peak at 14.5 to 15 MeV, so the peak energy of the measured spectrum is slightly low, which would be caused by improper energy calibration. The fine structure at the several mega-electron-volt region that appeared in the measured value was not observed in the calculation. The reason for such discrepancy was mainly the uncertainty in the unfolding method.[10] To discuss the discrepancy in detail, we may

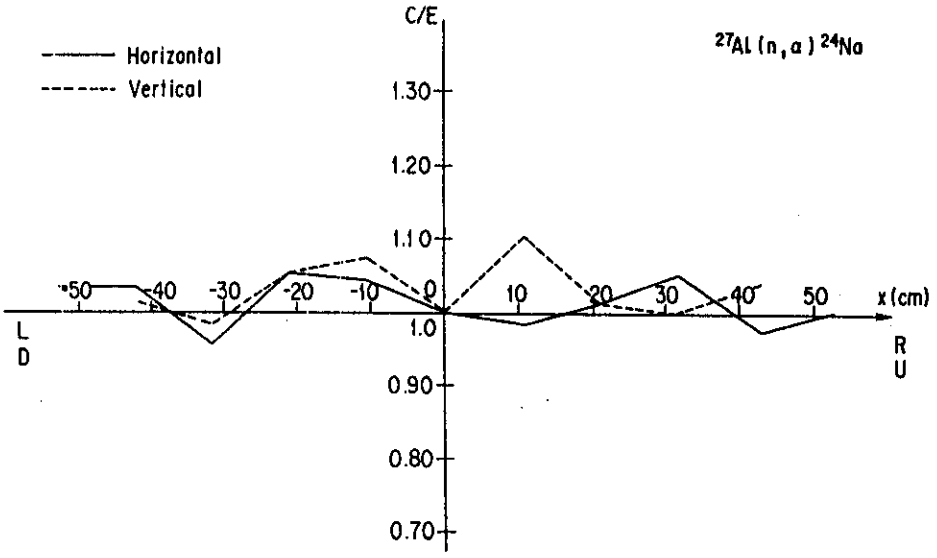

Fig. 12. The C/E values for the $^{27}Al(n,\alpha)^{24}Na$ reaction rate; $x = y = 0$ is the center of the test region surface.

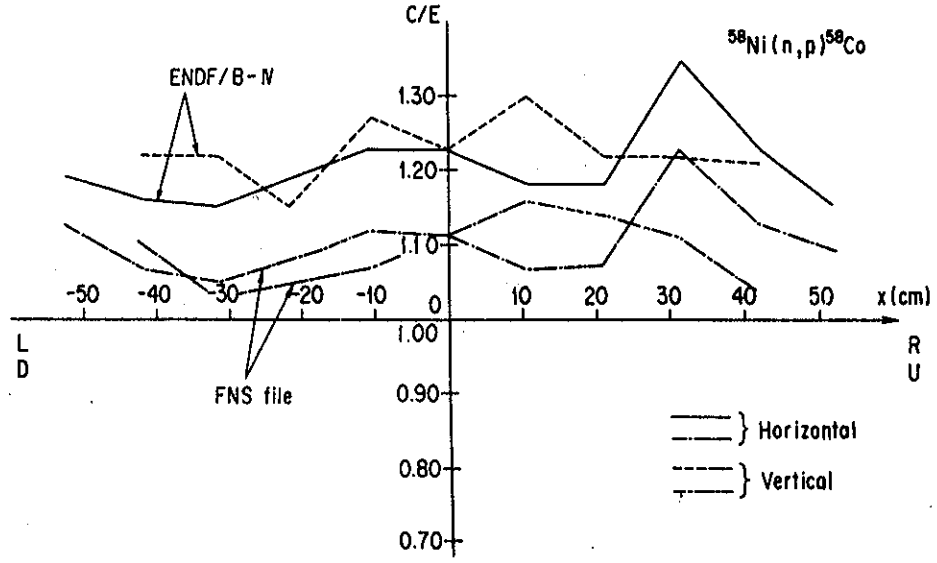

Fig. 13. The C/E values for the $^{58}Ni(n,p)^{58}Co$ reaction rate; $x = y = 0$ is the center of the test region surface.

need more accurate measurements by a neutron time-of-flight method. Figure 19 compares the calculation and the measurement by NE-213 and PRC. Both results agree within the statistical uncertainty of the Monte Carlo calculation below 1 MeV. The peak that appeared at ~800 keV in the PRC measurement corresponds to protons from the $^3He(n,p)$ reaction, and accordingly, it does not appear in the calculated spectrum. The dip and the peak at ~30 keV are due to the resonance of iron, which was the first-wall material. Because the resonance self-shielding effect was not considered in the calculation, the resonance structure was overestimated. In Fig. 20, the U.S. results by DOT5.1 and MATXS6 are compared with the same measurement. The general trend of agreement between the calculation and the measurement was similar to the one by JAERI. The self-shielding effect on resonances was not taken into account in the U.S. calculations. The calculations can predict well the measured spectrum except for the several mega-electron-volt region. The resolution of the measurement is not good enough to separate the fine structure due to resonances.

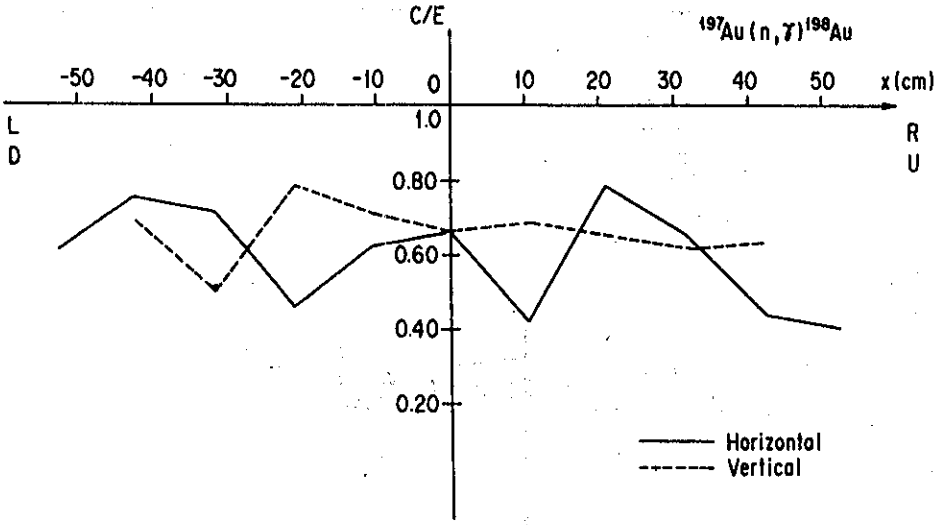

Fig. 14. The C/E values for the $^{197}Au(n,\gamma)^{198}Au$ reaction rate.

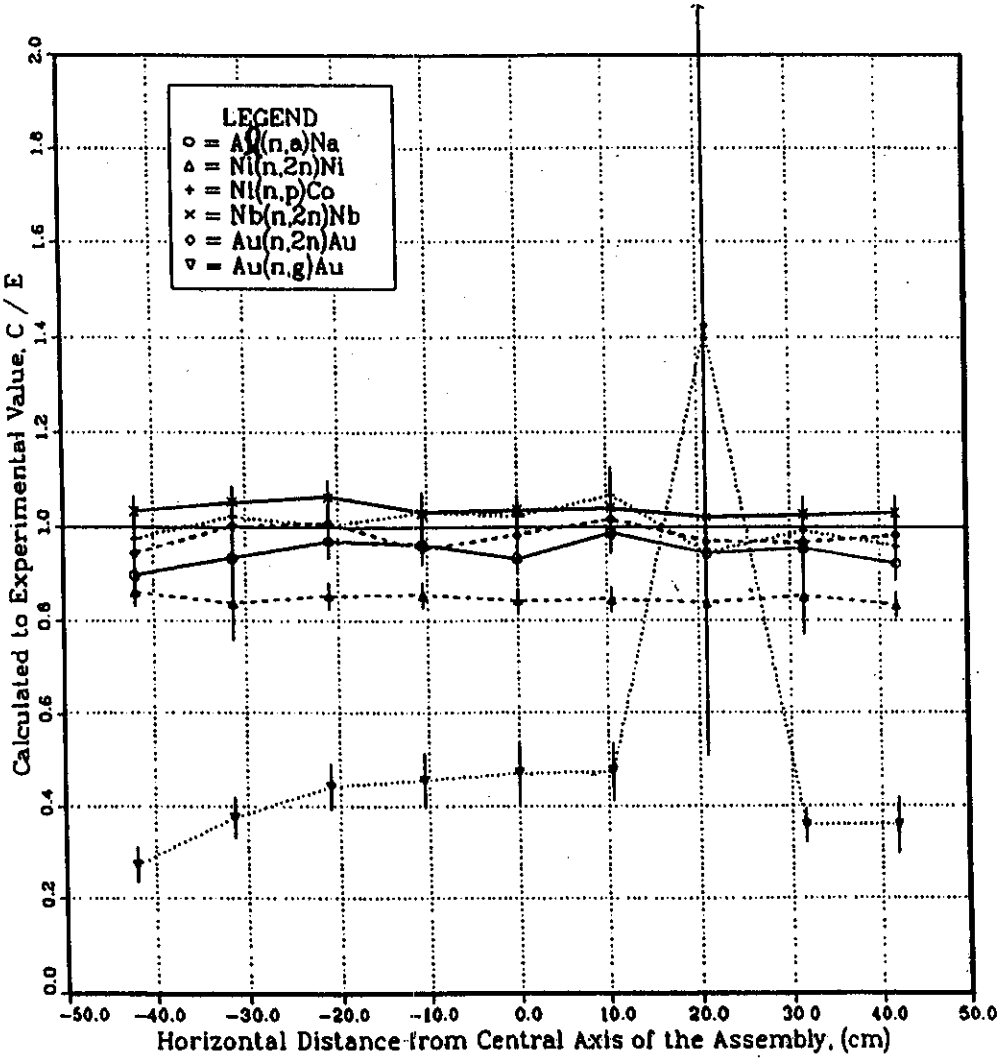

Fig. 15. The C/E values of the reaction rates at the front surface of the Phase-IIA reference system (horizontal distribution).

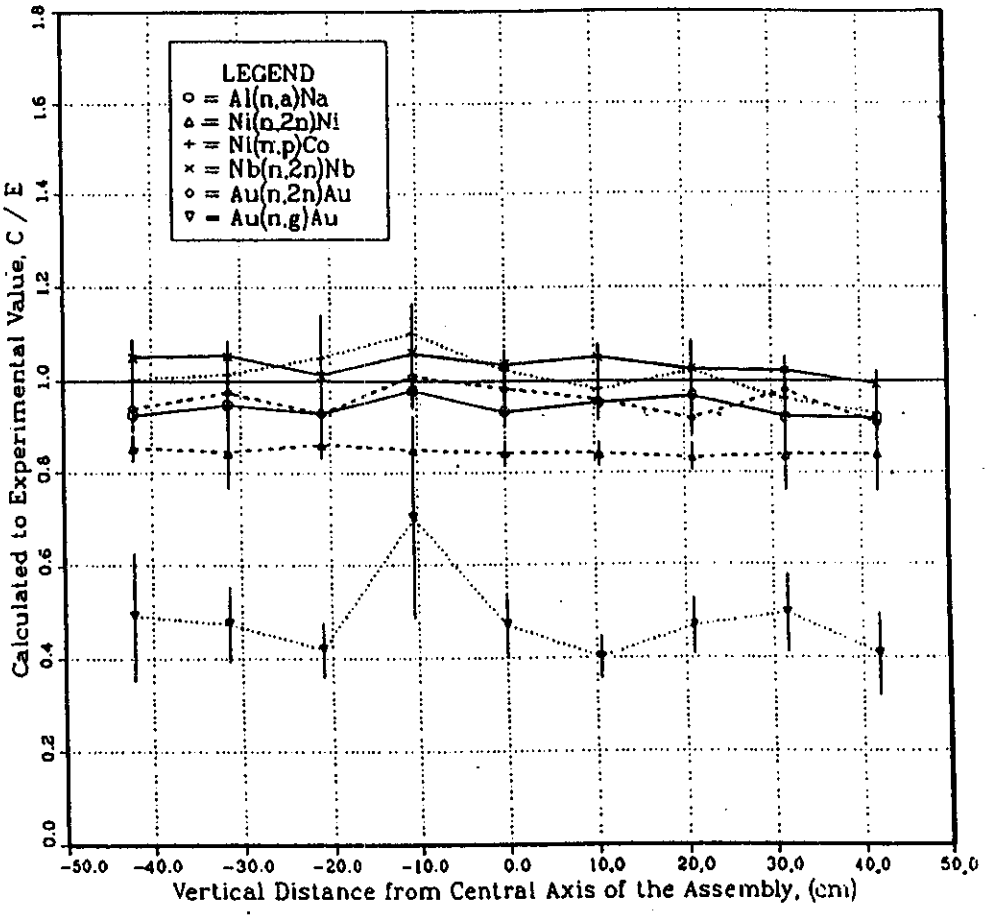

Fig. 16. The C/E values of the reaction rates at the front surface of Phase-IIA reference system (vertical distribution).

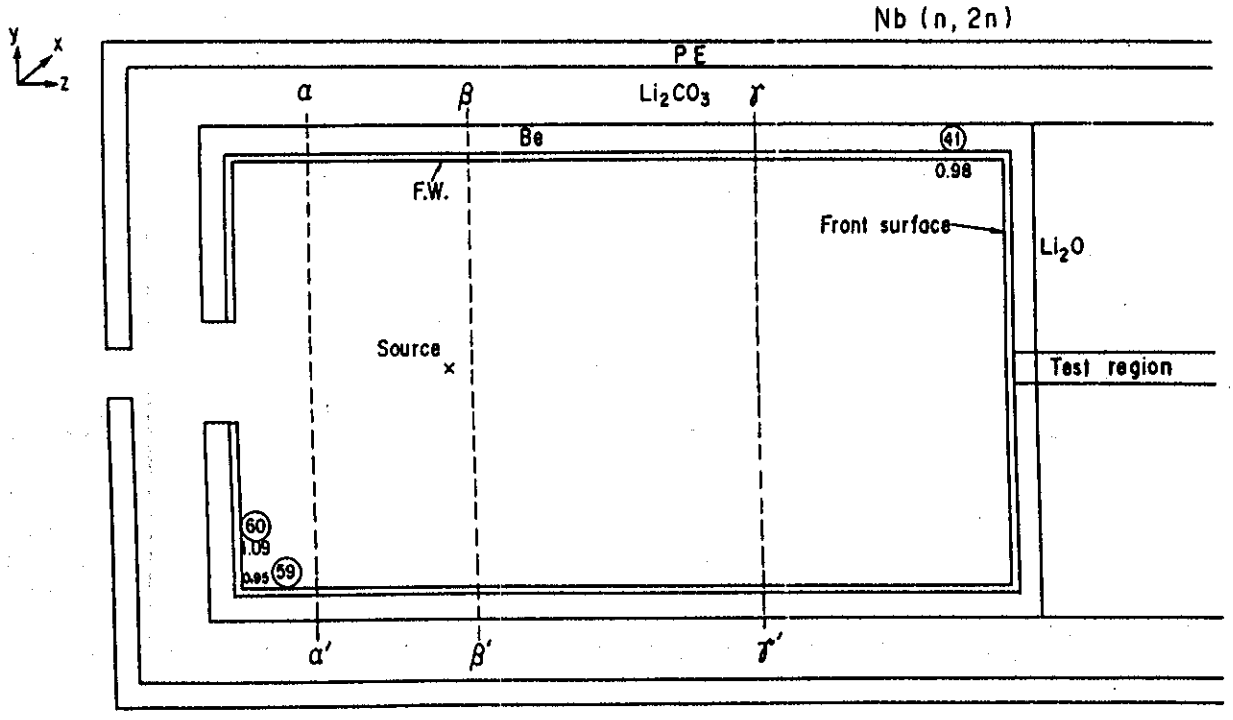

Fig. 17. The positions of the reaction rate measurements using activation foils.

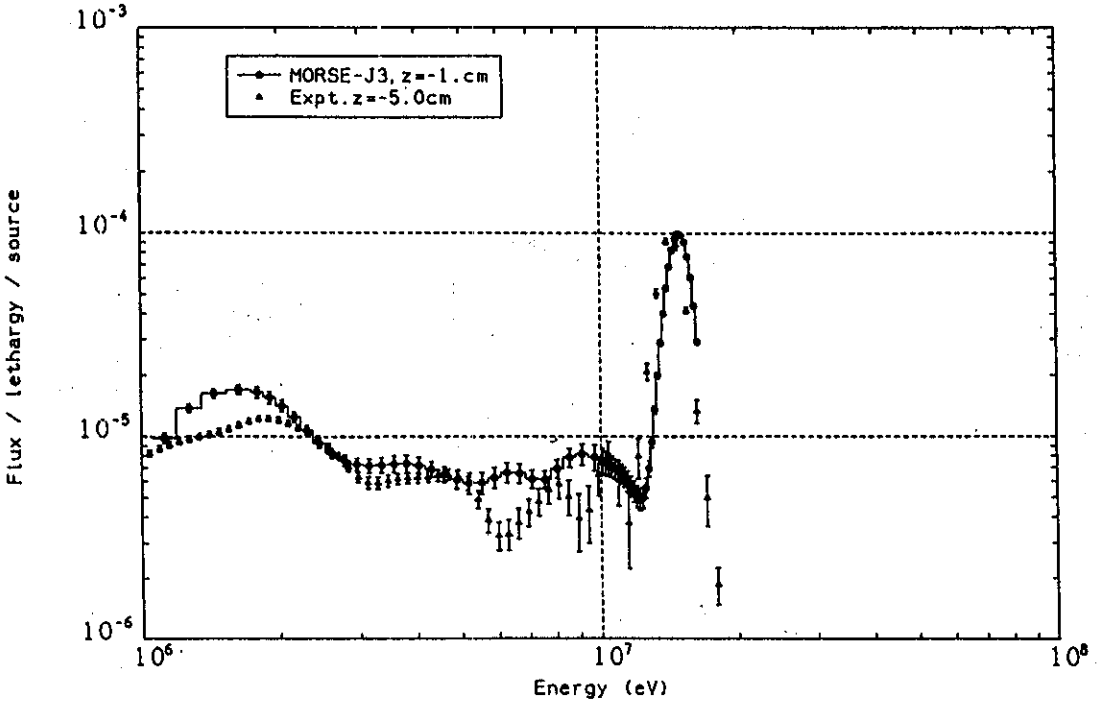

Fig. 18. The neutron spectrum above 10 MeV at the front surface of the test region in the Phase-IIB system.

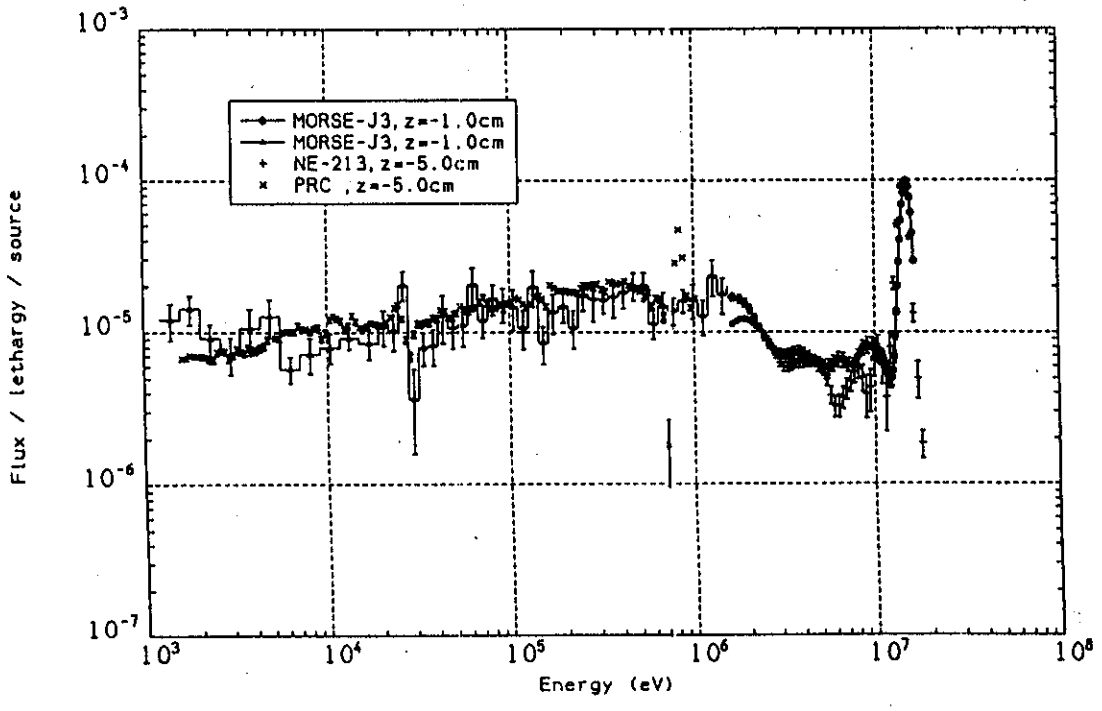

Fig. 19. The neutron spectrum above 1 keV at the front surface of the test region in the Phase-IIB system.

The C/E values for the Nb(n,2n) reaction rates are shown in Figs. 21 and 22, where the U.S. results are shown in parentheses. The C/E values by JAERI at the $\alpha - \alpha'$ cross section (the backward direction of RNT) are close to unity except for the foils 29, 32, and 36, and the U.S. values are higher by ~10%. Those by JAERI at the $\beta - \beta'$ cross section (close to the source generation point in RNT) are smaller by 10 to 20% than unity

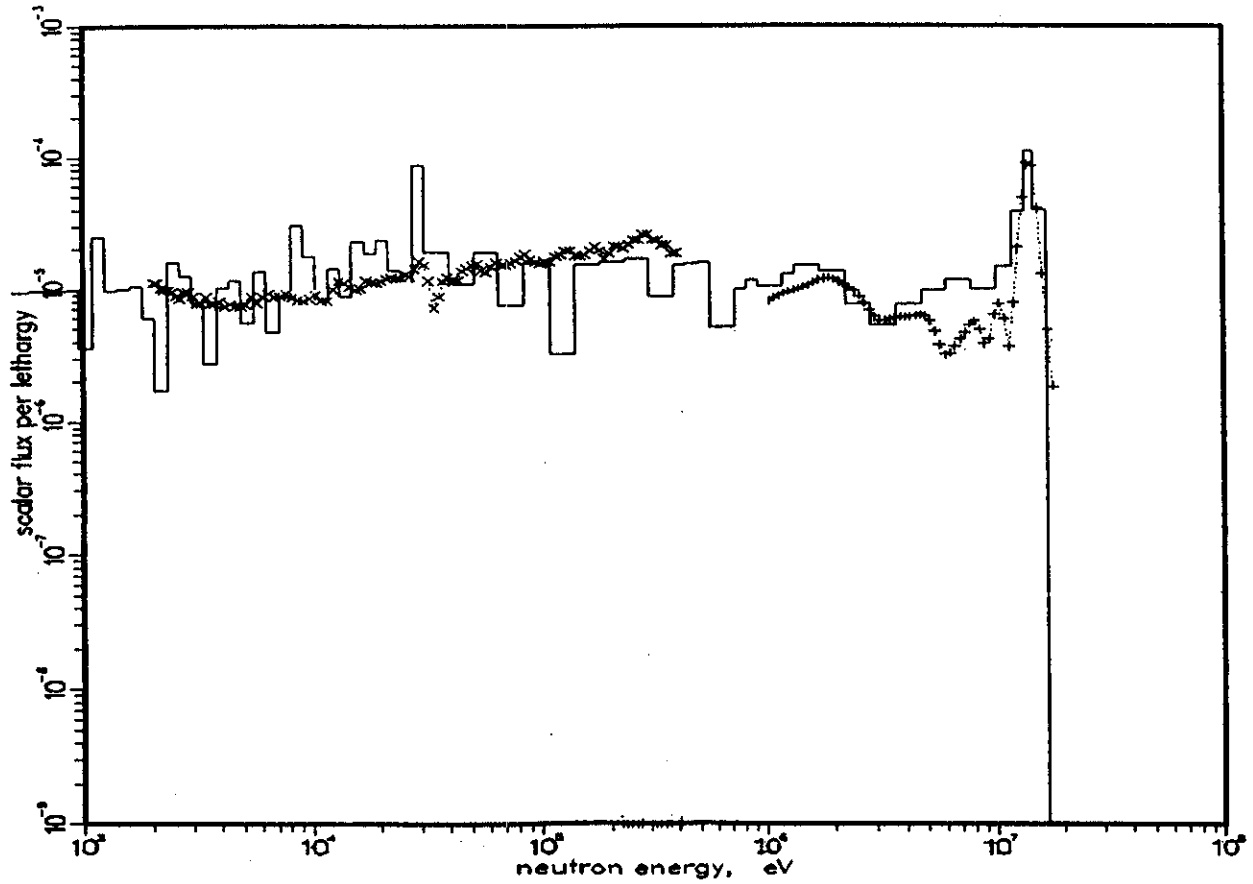

Fig. 20. The U.S. result of the neutron spectrum above 1 keV at the front surface of the test region in the Phase-IIB system (+ represents NE-213, and × represents PRC).

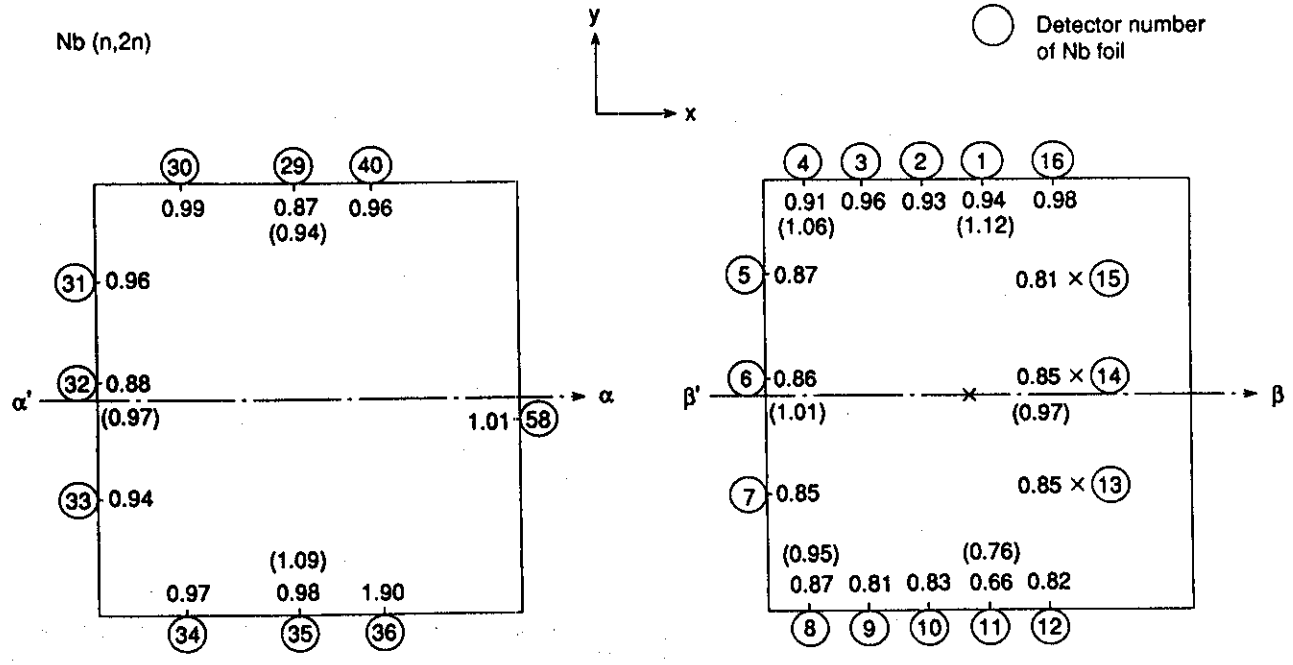

Fig. 21. The C/E map of the $^{93}Nb(n,2n)^{92}Nb$ reaction rates on the vertical cross sections $\alpha - \alpha'$ and $\beta - \beta$ in the Phase-IIB system.

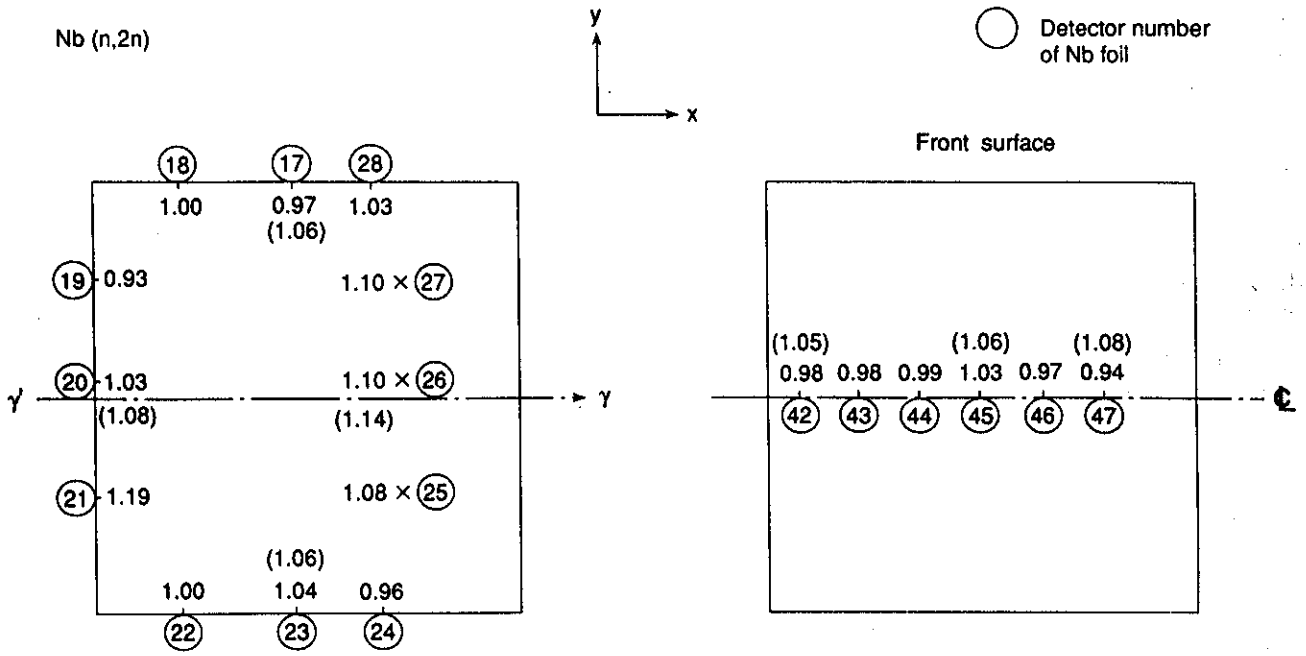

Fig. 22. The C/E map of the $^{93}Nb(n,2n)^{92}Nb$ reaction rates on the vertical cross sections $\gamma - \gamma'$ and the test region surface in the Phase-IIB system.

while those by the United States are higher by 10 to 15% than those by JAERI. At these foil locations (1 through 16), neutrons generated at the source point contributed to reactions after colliding with the complex structure materials of RNT, and hence, the accuracy in modeling significantly affected the calculated values. The present model caused neutrons emitted in the vertical direction to suffer more collisions with RNT than the real case, and the U.S. model gave better agreement. In the forward region from RNT, the reaction rates could be well predicted, as shown in Fig. 22. On the $\gamma - \gamma'$ cross section, the agreement was generally good, although the calculations overestimated by 10% positions 25 and 27 and the U.S. results gave the larger C/E values by several percent. Such discrepancies would be caused by modeling the experimental condition. At the front surface, the agreement was very good, although the U.S. results overestimated several percent.

From the analysis of the source characteristics mentioned earlier, the incident neutrons in the test region could be well predicted by the present method above a few kilo-electron-volt energy region. The modeling of RNT sensitively affects the calculated reaction rates at the back and the neighborhood of the target. A prediction accuracy below the kilo-electron-volt region could not be examined, although a considerable number of neutrons will exist in the low-energy region because the cavity is surrounded by a good reflective material, beryllium.

V. SUMMARY

The neutron current in the Li_2O test region consists of the direct component from RNT and the scattering component from the container or the test region. Because the influence from the experimental room wall was negligibly small in the Phase-II assembly, source characteristics were analyzed for only the assembly. Observations derived from the analysis are summarized as follows:

1. Neutron spectra above a few kilo-electron-volts and reaction rates by activation foils can be satisfactorily predicted by the current transport codes, the recently evaluated nuclear data, and the calculation models.

2. With respect to neutron spectra of the Phase-IIA system, integrated spectra above 10 MeV agree well with the measured spectra while the discrepancy of a few tens of percent is observed in the range of 1 to 10 MeV.

3. Below 1 MeV, both spectra by MORSE-DD and DOT5.1 agree generally well with the measurements by PRC except for the fine structure due to scattering resonances.

4. The prediction accuracy of the activation rates depends on the activation cross sections used. The ENDF/B-IV and ENDF/B-V underestimate the $Ni(n,2n)$ reaction rate by 10 to 15% and overestimate the $Ni(n,p)$

reaction rate by 10 to 20% while recently evaluated nuclear data can significantly reduce discrepancies. However, the Ni(n,2n) cross section in the ACTL library is not appropriate. In conclusion, the threshold reaction rate can be predicted within ±10% if recent nuclear data are used.

5. Although discrepancies were observed in the few back locations of RNT, these hardly influence the prediction accuracy of the incident neutron current in the test region.

6. In the Phase-IIB experiment, the Nb(n,2n) activation rates were measured at three vertical cross sections and on the surface of the test region. The trend of the C/E values is similar to the cases of the Phase-IIA measurement. The characteristics of the incident neutrons in the test assembly is confirmed to be well predicted, although there is some problem in the measurement of the neutron spectrum by NE-213.

7. Because the cavity region is surrounded by a good reflective material of beryllium for Phase-IIB, a considerable number of neutrons will exist in the low-energy region below kilo-electron-volts, but such a component cannot be well examined in the present experiments.

REFERENCES

1. M. NAKAGAWA et al., "JAERI /U.S. Collaborative Program on Fusion Blanket Neutronics—Analysis of Phase IIA and IIB Experiments," JAERI-M 89-154 (1989).

2. M. Z. YOUSSEF et al., "U.S./JAERI Collaborative Program on Fusion Neutronics, PhaseIIA and IIB Fusion Integral Experiments," UCLA-ENG-90-14, FNT-31, University of California, Los Angeles (1989).

3. K. SHIBATA et al., "Evaluation of Nuclear Data of ^{6}Li for JENDL-3," JAERI-M 84-198, Japan Atomic Energy Research Institute (1984); see also "Evaluation of Neutron Nuclear Data of ^{7}Li for JENDL-3," JAERI-M 88-204, Japan Atomic Energy Research Institute (1984).

4. Y. IKEDA et al., "Activation Cross Section Measurements for Fusion Reactor Structural Material at Neutron Energy from 13.3 to 15.0 MeV Using FNS Facility," JAERI 1312, Japan Atomic Energy Research Institute (1988).

5. T. MORI, M. NAKAGAWA, and M. SASAKI, "One-, Two-, Three- Dimensional Transport Code Using Multigroup Double Differential Cross Sections," JAERI 1314, Japan Atomic Energy Research Institute (1988).

6. LOS ALAMOS MONTE CARLO GROUP, "A General Monte Carlo Code for Neutron and Photon Transport, Version 3A," LA 7396, Rev. 2, Los Alamos National Laboratory (1986).

7. R. A. MacFARLANE, "TRANSX-CTR: A Code for Interfacing MATXS Cross Section Libraries to Nuclear Transport Codes for Fusion Systems Analysis," LA 9863, Los Alamos National Laboratory (1984).

8. J. BENVENISTE et al., "Information on the Neutrons Produced in the ^{3}H(d,n)^{4}He Reaction," UCRL-4266, University of California, Los Angeles (1954).

9. J. BENVENISTE et al., "The Problem of Measuring the Absolute Yield of 14 MeV Neutrons by Means of an Alpha Counter," *Nucl. Instrum. Methods*, 7, 306 (1960).

10. Y. OYAMA et al., "Design and Techniques for Fusion Blanket Neutronics Experiments Using an Accelerator-Based Deuterium-Tritium Neutron Source," *Fusion Technol.*, **28**, 56 (1995).

Masayuki Nakagawa (BS, 1965; MS, 1967; and PhD, 1979, nuclear engineering, Kyoto University, Japan) is a principal scientist in the Department of Reactor Engineering at the Japan Atomic Energy Research Institute (JAERI). He is a head of the reactor system laboratory having the main responsibility for the computation method and design of reactors. He researched the development of neutronics computation methods and codes for fast reactors and fusion reactors and intelligent reactor design systems. His group has developed high-speed general-purpose Monte Carlo codes based on vector and/or parallel algorithms.

Takamasa Mori (BS, 1976; MS, 1979; and PhD, 1985, nuclear engineering, Kyoto University, Japan) is a principal scientist in the Department of Reactor Engineering at JAERI. He worked for the development of neutron transport codes using double-differential form cross sections. His research interests are in the field of reactor physics, especially the speedup of Monte Carlo calculation of high-energy particles based on vector and/or parallel algorithms.

Kazuaki Kosako (BE, atomic engineering, Tokai University, Japan, 1984) has worked at Sumitomo Atomic Energy Industries since 1994. He worked in the Department of Reactor Engineering at JAERI from 1984 to 1992 where

he was involved mainly in fusion neutronics. He is currently interested in the area of radiation damage of materials.

Yukio Oyama (BS, physics, 1975; MS, nuclear physics, 1977; and Dr. Eng., 1989, Osaka University, Japan) is a principal scientist at JAERI. He has worked in the area of fusion neutronics experiments since 1978. He is currently involved in intense and high-energy neutron source projects.

Yujiro Ikeda (PhD, nuclear engineering, Nagoya University, Japan, 1981) is head of the Fusion Neutronics Laboratory in the Department of Reactor Engineering at JAERI. He has worked in the areas of fusion neutronics experiments, induced radioactivity experiment and analysis, direct nuclear heating measurements, activation cross-section measurements, and fusion dosimetry.

Chikara Konno (MS, physics, Kyoto University, Japan, 1985) is a research scientist in the Department of Reactor Engineering at JAERI. He has worked in the areas of fusion neutronics experiments, cross-section measurements, and neutron spectrum measurements using a proton-recoil counter.

Hiroshi Maekawa (BE, 1965; MS, 1967; and Dr. Eng., 1970, nuclear engineering, Tokyo Institute of Technology, Japan) is the deputy director of the Department of Reactor Engineering and the head of the Intense Neutron Source Laboratory at JAERI. He has worked on fusion neutronics for more than 20 years, and he planned and constructed the Fusion Neutronics Source facility. He served as the Japanese leader of the JAERI/U.S. Department of Energy (U.S. DOE) collaboration on fusion blanket neutronics. His recent research has focused on International Fusion Materials Irradiation Facility conceptual design activities.

Tomoo Nakamura (BS, physics, Kyoto University, Japan, 1957) is currently director of the Public Acceptance Database Center, Research Organization for Information Science and Technology. His research background includes experimental reactor physics on fast breeder reactors and nuclear technology on fusion reactor blankets. He served as the former Japanese leader of the JAERI/U.S. DOE collaboration on fusion blanket neutronics.

Mohamed A. Abdou is a professor in the Department of Mechanical, Aerospace, and Nuclear Engineering at the University of California, Los Angeles (UCLA) and also is the director of fusion technology at UCLA. His research interests include neutronics, thermomechanics, fusion technology, and reactor design and analysis. He served as the U.S. leader of the JAERI/U.S. DOE collaboration on fusion blanket neutronics.

Edgar F. Bennett (PhD, University of New Hampshire, 1957) is a physicist at Argonne National Laboratory (ANL). He has been a section head of experimental reactor physics since 1970. He is best known as the inventor of a widely used in-core proton-recoil spectrometer—a technique that he has been continually updating. He has also made contributions to the field of reactivity measurement by reactor noise techniques, in particular, by providing a common theoretical basis and introducing a new type of variance experiment.

Mahmoud Z. Youssef (PhD, nuclear engineering, University of Wisconsin, 1980) is a senior research engineer in the Department of Mechanical, Aerospace, and Nuclear Engineering at UCLA. He participated in several conceptual magnetic fusion energy and inertial fusion energy reactor design studies with emphasis on nuclear analysis and blanket/shield design. His research interests are in the areas of blanket/shield design optimization, nuclear data, sensitivity/uncertainty studies, neutronics methods and code development, tritium fuel cycle, radioactivity and safety aspects of fusion, integral experiments, neutronics testing, and research and development for fusion reactors, particularly the International Thermonuclear Experimental Reactor (ITER).

T. Yule (BS, physics, John Carroll University, 1962; MS, physics, University of Wisconsin, 1964; PhD, nuclear physics, University of Wisconsin, 1968) is a physicist and program manager in the Technology Development Division at ANL. His specialties include nuclear applications, experimental reactor physics, accelerator engineering, radiological health physics, and aerosol science.